

## Onset of a collisional modification of the Faraday effect in a high-density atomic gas

M. Kristensen, F. J. Blok, M. A. van Eijkelenborg, G. Nienhuis, and J. P. Woerdman  
*Huygens Laboratory, University of Leiden, P.O. Box 9504, 2300 RA Leiden, The Netherlands*

(Received 5 July 1994)

We investigate, theoretically and experimentally, the onset of modified electronic precession due to quasimolecular behavior in dense atomic gases. The close connection between the angular coupling of collision pairs and a modification of the Faraday effect is pointed out. We have observed the onset of this quasimolecular modification of the atomic Faraday effect with high-resolution laser measurements of the absorption and Faraday spectra near the  $D_2$  line of Rb atoms immersed in high-density buffer gases. The atomic Faraday effect itself is also affected by the presence of nuclear spin; this modifies the electronic precession through angular-momentum coupling. We describe how to separate the effect of nuclear spin from the effects due to quasimolecular behavior. In this way we establish the existence of angular coupling of the Rb valence electrons to neighboring buffer-gas atoms at densities above  $\sim 2 \times 10^{19} \text{ cm}^{-3}$  in Xe buffer gas. In He buffer gas, quasimolecular modifications of the Faraday effect are approximately two times smaller than for Xe.

PACS number(s): 32.70.-n, 78.20.Ls, 32.90.+a

### I. INTRODUCTION

When a light beam passes through matter under the influence of a magnetic field its state of polarization changes. Such magneto-optic effects are well understood for the case of dilute atomic gases where there is no interaction between the individual atoms. For molecular systems the polarization effects are more complicated, but it is still helpful to use information from magneto-optical studies for investigating molecular structure [1]. Our understanding is even more incomplete for condensed-matter systems because the atomic interactions play a dominant role. In this paper we investigate the initial part of the transition from a dilute gas to condensed matter and try to improve our understanding of the onset of complexity in magneto-optical spectra. We show how information obtained in this transition region may improve our knowledge of the atomic interactions involved. In this way studies of magneto-optic effects can be used to probe collisional physics; conversely, results obtained from collision experiments can be used to predict magneto-optical effects. Therefore our results may prove valuable both for spectroscopists and collisional physicists. Also diagnostic aspects may be involved since magneto-optic effects are sometimes used for density measurements [2,3].

We will limit our studies to the Faraday effect which occurs when nonsaturating, linearly polarized light near an atomic resonance frequency passes through matter in a longitudinal magnetic field. This does not imply a loss of generality since other magneto-optical effects such as magnetic circular dichroism are related to the Faraday effect through Kramers-Kronig transformations [1]. The Faraday rotation angle

$$\theta_{\text{Far}} = \frac{\pi \nu L}{c} (n_- - n_+) \quad (1)$$

arises from the difference in refractive indices  $n_+$  and  $n_-$

for the two opposite circular polarizations. In Eq. (1)  $\nu$  is the optical frequency,  $L$  the length of the sample, and  $c$  the velocity of light. The Faraday effect has been studied intensively for many different systems. For a dilute atomic gas the Faraday rotation angle  $\theta_{\text{Far}}$  is proportional to the dispersion  $dn/d\nu$ , as expected from classical electrodynamics. This result is called the Becquerel relation [4-6]

$$\theta_{\text{Far}} = \theta_{\text{Becq}} = \alpha \frac{e}{2mc} BL \nu \frac{dn}{d\nu}, \quad (2)$$

where  $-e$  is the electron charge,  $m$  is the electron mass,  $B$  is the longitudinal magnetic field, and  $\alpha=1$  in a classical system (spinless atomic state). The first obvious complication of this classical description of the Faraday effect is the presence of spin in most atoms. Both the electron spin and the nuclear spin must be considered. Quantum mechanically, Eq. (2) remains valid for optical transitions in the presence of spin only if we deal with *isolated* lines. In this case the atomic levels involved have well-defined  $g$  factors ( $\neq 1$ ) generally leading to  $\alpha \neq 1$  in Eq. (2) [5,6]. As a side result of this paper, we will show that the Becquerel relation remains valid in a formal sense for overlapping lines, with generally different Zeeman splittings, if  $\alpha$  and  $dn/d\nu$  are replaced by tensorial quantities. This is called the generalized Becquerel relation.

For molecular systems the Faraday effect is substantially more complicated than for atoms due to their internal structure [7] and violations of the generalized Becquerel relation can be observed [8]. For polyatomic molecules with low symmetry the  $g$  factors are virtually impossible to understand in simple physical terms [1]. Even in diatomic molecules perturbations are often present, leading to state mixing. This may selectively change molecular  $g$  factors for one or several lines in a rotational band due to accidental degeneracies. For condensed matter the complications are always more severe than for molecules because atomic states merge to form a band

structure and most interactions are nonbinary in nature. It is therefore difficult to find detailed relations between the internal structure and the Faraday effect. This difference from the dilute gas can generally be seen as a breakdown of the single-atom picture necessary for the validity of the Becquerel relation.

The onset of violations of the Becquerel relation has been predicted for atomic gases at densities sufficiently high that the broadening of an optical transition cannot be described within the impact approximation, even close to line center [5]. Classically, this can be seen as the modification of electronic precession in a magnetic field when the electron experiences an anisotropic potential. We have recently confirmed this prediction for the special case of Rb atoms perturbed by Xe buffer gas at  $\sim 6 \times 10^{19} \text{ cm}^{-3}$  [9]. In the present paper we give a complete account of the connection between the absorption and the Faraday effect of Rb atoms in He and Xe buffer gases up to densities of  $\sim 10^{20} \text{ cm}^{-3}$  and compare the experimental results with a theoretical model including the effects of spin, in particular, nuclear spin. The inclusion of nuclear-spin effects is conceptually simple, but technically complicated. This inclusion, however, is unavoidable for understanding the onset of quasimolecular effects for alkali-metal–noble-gas systems. Due to their one-electron nature these extensively studied systems are the most promising candidates for establishing direct connections between experiment and theory.

The choice of Rb in He and Xe buffer gases as an experimental system is motivated as follows. First of all, the wavelengths of the Rb fine-structure transitions are convenient to reach with commercially available semiconductor lasers. Only the  $D_2$  transition is of immediate interest since no deviations from the Becquerel relation are expected theoretically for the  $D_1$  transition because both the lower state ( $^2S_{1/2}$ ) and the upper state ( $^2P_{1/2}$ ) are spherically symmetric [10]. This spherical nature prevents electronic anisotropy unless fine-structure mixing becomes important. Second, the electronic anisotropy of the Rb noble-gas interaction  $V_\Sigma - V_\Pi$  is large for the highly polarizable Xe atoms leading to an enhancement of the angular coupling [9]. Here  $\Sigma$  refers to the  $^2\Sigma_{1/2}$  level and  $\Pi$  to the  $^2\Pi_{3/2}$  level in the upper state  $^2P_{3/2}$  involved in the  $D_2$  transition. We will later show in detail [see Eq. (30)] that the angular coupling effect gets further exacerbated by the low relative velocity  $v$  for the Rb:Xe system, as compared to other alkali-metal–noble-gas systems. These qualitative predictions of the dependence of angular coupling on atomic properties agree with the experimental findings when we compare the He and Xe results. Finally, for Rb there is a large fine-structure splitting of the  $D_1$  and the  $D_2$  transitions which helps simplify the theoretical interpretation because it greatly reduces fine-structure mixing. Without fine-structure mixing the only effect of the electron spin is to change the angular momentum coupling, giving rise to different values of  $\alpha$  in Eq. (2) for the  $D_1$  and  $D_2$  transitions. For the  $D_1$  transition we find  $\alpha = \frac{4}{3}$  and for the  $D_2$  transition we find  $\alpha = \frac{7}{3}$  [5,6].

Theoretically, the detailed connection between the adi-

abatic potentials and gas-phase spectra is made by spectral line-broadening theories. The most advanced of these, the so-called unified line-broadening (ULB) theory [11], describes the full shape of the line, reducing to the quasistatic theory in the far wings and the impact theory at the line core. This theory holds as long as the duration of a collision  $\tau$  is short as compared with the mean time between successive collisions. This corresponds to the binary collision approximation. We have extended the ULB theory by incorporating the effect of a magnetic field, to describe magneto-optical spectra. We show that the effects of hyperfine structure can also be directly included in the ULB theory. The theoretical results are compared with our measurements on Rb atoms in both He and Xe buffer gases.

The structure of the article is as follows. In Sec. II we give an outline of the experimental method and describe the analysis to obtain the Becquerel violation from the measured absorption spectra and Faraday spectra. In Sec. III we give the line-broadening theory background necessary to disentangle the quasimolecular effects from effects of nuclear spin. In Sec. IV this theoretical model is compared with the experimental results and characteristic parameters describing the quasimolecular effects are extracted by fitting the model to the deviations from the Becquerel relation. In Sec. V we introduce a qualitative microscopic model which allows us to discuss the results in terms of collisional properties of the Rb:He and Rb:Xe systems. In Sec. VI we draw conclusions. Readers who are more interested in the collisional physics than in line broadening may proceed with Sec. IV directly after Sec. II.

## II. EXPERIMENT

Figure 1 shows our experimental setup. The frequency of a semiconductor laser is current tuned over the pressure-broadened Rb line. Using different laser temperatures it is possible to cover more than 600 GHz, without mode hopping, with two selected Hitachi HL7838G lasers. A small fraction of the light output is in side modes, below lasing threshold, positioned at integer multiples of 150 GHz from the main lasing mode. This fraction is filtered out with a monochromator which defines a frequency window of  $\sim 40$  GHz full width at half maximum (FWHM). The individual laser scans, of  $\sim 40$  GHz each, are linearized along the frequency axis using interferometer fringes for calibration. Absolute frequency calibration is made with vacuum cells filled with Rb and  $I_2$ , which also allow us to correct for effects of long-term laser drift and to join individual laser scans together to form complete spectra.

As the sample cell we use a 4-cm-long glass vessel filled with Rb metal and noble buffer gas. In order to reduce étalon effects the cell windows are wedge shaped with an angle of  $2^\circ$  between their surfaces and they are antireflection coated on the outside (residual reflectivity  $< 1\%$ ). We operate the cell at temperatures near  $T \approx 350$  K, which gives a saturated Rb vapor density  $N_{\text{Rb}} \approx 10^{12} \text{ cm}^{-3}$ . A typical buffer gas density is  $2 \times 10^{19} \text{ cm}^{-3}$  ( $\sim 1$

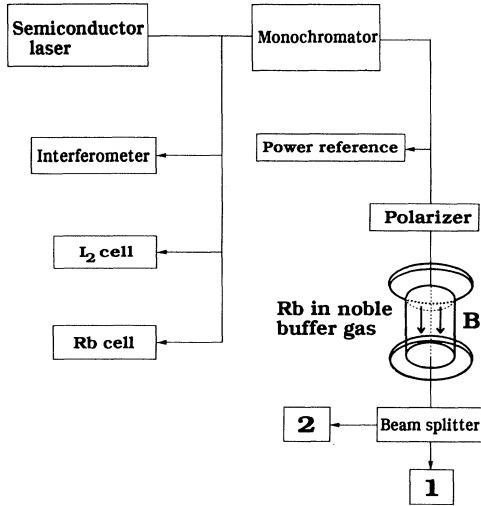


FIG. 1. Experimental setup to measure the Faraday spectrum and absorption spectrum of Rb atoms immersed in a noble gas. The gas cell is surrounded by two coils that can produce a solenoid magnetic field up to 0.03 T. The arrows indicate one of the two possible directions of the magnetic field  $B$ .

atm at 350 K) corresponding to  $\sigma \approx 7$  GHz, where  $\sigma$  is the frequency half width at half maximum of the absorption curve [12]. Under these conditions we have approximately one absorption length (63% absorption) at the center of the  $D_2$  line. For different buffer-gas densities we adjust the temperature to obtain again approximately one absorption length in the cell. Absorption beyond  $\sim 85\%$  increases the influence of systematic errors and of shot noise; the latter is our most important noise limitation at low laser power.

The transmission and Faraday spectra are recorded simultaneously in a balanced bridge configuration. A longitudinal magnetic field of up to  $B \approx 0.03$  T is supplied by two coils with soft iron pole pieces for concentrating the flux. A polarizing beam splitter is oriented at about  $45^\circ$  relative to the incoming polarization to obtain equal intensities  $I_1$  and  $I_2$  at the two photodiodes 1 and 2 for the case  $B = 0$ . By suitably switching the magnetic field between  $B$  and  $-B$  at  $\sim 1$  Hz we obtain the Faraday rotation spectrum  $\theta_{\text{Far}}$  from

$$\theta_{\text{Far}} = \frac{1}{2}[\theta(B) - \theta(-B)], \quad \theta(B) = \frac{1}{2} \arcsin \left[ \frac{I_2 - I_1}{I_1 + I_2} \right]. \quad (3)$$

The transmission spectrum is obtained from  $I_1 + I_2$ , after normalization to the laser intensity passing through the monochromator.

If we choose  $L$  equal to one absorption length and tune the laser to the center of the absorption line we expect  $\theta_{\text{Far}} \sim \nu_L / (2\sigma)$  [5], where  $\nu_L \approx 0.5$  GHz is the Rb Larmor frequency at  $B = 0.03$  T. Therefore we have to measure rotations of the order of  $4 \times 10^{-2}$  rad at line center. For smaller buffer-gas densities we reduce the magnetic field to remain near this value. Larger magnetic rotation will

lead to measurable systematic errors due to the Paschen-Back effect in the ground-state hyperfine structure (this effect is not accounted for in our theory in Sec. III). Another important consideration is that for large Faraday rotations there will be some entanglement of the Faraday effect and circular dichroism; this is well known as the ultimate limiting factor in the performance of an optical Faraday isolator [13].

The dispersion spectrum is calculated from the absorption spectrum using Kramers-Kronig transformation. This is much more convenient than a direct measurement of the dispersion, which demands interferometric stability of the setup. The transformation procedure assumes linearity of the absorption and is therefore only correct if there is no optical hyperfine pumping. Saturation is negligible because of the large linewidth. Due to the high buffer-gas densities, diffusion in the cell is very slow and we estimate that it takes  $\sim 1$  s before a Rb atom is replaced by a spin-relaxed one from the cell wall. Therefore it may be expected that optical pumping effects only become negligible when every atom absorbs less than one photon per second. This occurs at a power level around 1 nW. In Fig. 2(a) we show the results of an experimental investigation of the optical pumping for Rb atoms in He buffer gas at 2 atm. We have plotted the ratio of the maximum value of the Faraday curve  $A$  relative to the average of the two local maxima  $B$  and  $C$  at the sides [see illustration in Fig. 2(c)] measured as a function of laser power. It is easy to see that this ratio is especially sensitive to optical pumping effects because the local maxima occur at the wings of the absorption curve where the individual hyperfine lines are pumped differently, while near line center the hyperfine lines are pumped almost

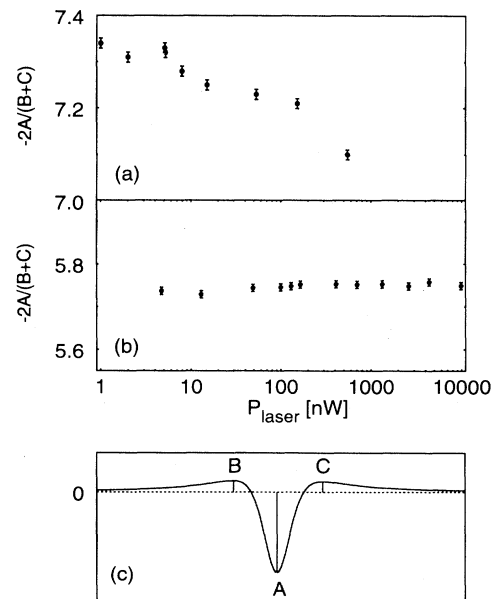


FIG. 2. Influence of optical pumping on the Faraday curves illustrated as the ratio between the local extremes as a function of laser power for (a) Rb:He and (b) Rb:Xe. (c) illustrates how to extract the ratio  $-2A/(B+C)$  from a Faraday spectrum  $\theta_{\text{Far}}(\nu)$ .

equally. From Fig. 2(a) we conclude that for He buffer gas it is safe to perform the experiments at 2 nW; for powers above  $\sim 100$  nW substantial optical pumping effects are observed. There might still be some small remaining effects ( $\sim 1\%$ ) of optical pumping below 2 nW, but these will be below our statistical measurement accuracy for the Faraday effect. For Xe buffer gas the situation is more favorable since the larger polarizability of Xe allows spin relaxation in the gas phase [14]. The influence of optical pumping for the Rb:Xe system is illustrated in Fig. 2(b), where the same ratio is plotted at 2 atm of Xe buffer gas. The absolute value is different for Xe and He buffer gases because of the different degree of line asymmetry (i.e.,  $B \neq C$  in Fig. 2). Experimentally we find no effect of optical pumping at 70 nW where we choose to perform the experiments in Xe buffer gas.

We obtain virtually shot-noise-limited detection for power levels of 10–100 nW with the balanced bridge detection method and modulation of the magnetic field. The main experimental uncertainty comes from alignment-dependent étalon effects in cell windows, polarizers, and other optical elements. Another uncertainty is due to uncontrolled variations of up to 1% in the absorption in the high-pressure cell, as a function of time, with typical time scales in the range 0.01–1 s. We suspect these to be due to the onset of weak convection in the cell. Generally, errors in the spectra increase with pressure because it becomes necessary to use more than one laser to cover the absorption spectrum and each laser change necessitates realignment. Particularly étalon effects get emphasized when the individual laser scans are joined to produce the final spectra; this gives rise to errors in the measured deviation from the Becquerel relation of up to 1% of the maximum value of the Faraday rotation for Rb:Xe and 2% for Rb:He (the lower laser power used for Rb:He makes precise alignment more difficult). Further experimental errors may result from the remaining laser output in side modes, leaking through the monochromator. We measured this leakage to be below 0.05% and therefore the consequences for the absorption and Faraday spectra must be of the same order of magnitude. Variations in offsets for our electronics were also of this order of magnitude. In the following we will therefore ignore these two types of errors.

After recording laser scans of the transmission and Faraday rotation spectra over a frequency range of at least 20 times FWHM we joined these together to form complete spectra using the iodine lines as frequency markers. We calculated the absorption spectrum by taking the logarithm of the observed transmission spectrum. Figure 3 illustrates some typical results obtained with Xe buffer gas. Figure 3(a) shows the absorption spectrum of the Rb  $D_2$  line obtained at  $[\text{Xe}] = 4.41 \times 10^{19} \text{ cm}^{-3}$  ( $T = 340 \text{ K}$ ,  $P_{\text{Xe}} = 2.05 \text{ atm}$ ). A clear shift and asymmetry are observed for the pressure-broadened spectrum as compared to the Rb spectrum in vacuum, which is also shown. The Rb vacuum spectrum consists of four lines; two hyperfine lines from each of the two isotopes  $^{85}\text{Rb}$  and  $^{87}\text{Rb}$ . The hyperfine structure of the upper state is not resolved. Figure 3(b) shows the measured corresponding Faraday spectrum. This spectrum is also shift-

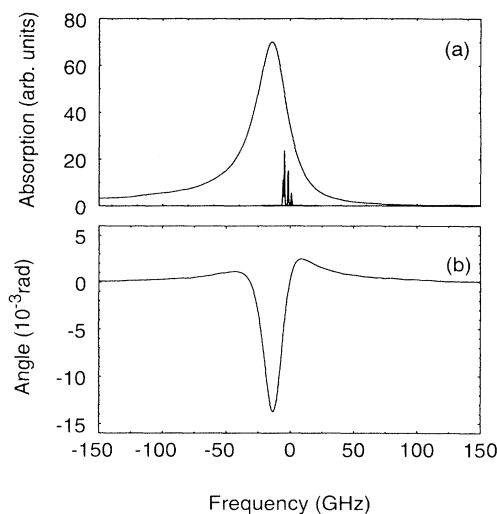


FIG. 3. (a) Absorption spectrum and (b) Faraday spectrum for the Rb  $D_2$  transition at  $[\text{Xe}] = 4.41 \times 10^{19} \text{ cm}^{-3}$ .

ed and asymmetric. In Fig. 3 we show only the central part of the spectra since this contains the interesting structure; for further analysis we used the complete spectra.

We performed a Kramers-Kronig transformation of the absorption spectrum and obtained the Becquerel spectrum by differentiation. As the Kramers-Kronig transformation includes an integration to infinity, we need some function for extrapolation in the far wings of the absorption spectrum. As the fitting and extrapolation function for the absorption curve  $\kappa(\nu)$  we used an asymmetric Lorentzian which has previously been used to fit pressure broadened absorption spectra [15],

$$\kappa(\nu) = A_a \sum_{j=1}^2 \sum_{i=1}^2 \frac{\beta_{ij}(1-\gamma X_{ij})}{1+X_{ij}^2} + B_a, \quad X_{ij} = \frac{\nu - \nu_{ij} - \delta}{\sigma}, \quad (4)$$

where the  $i$  summation is over the two resolved hyperfine lines and the  $j$  summation is over the two isotopes  $^{85}\text{Rb}$  and  $^{87}\text{Rb}$  with the natural abundances 72.15% and 27.85%. As explained in Sec. III, the use of a Lorentzian with a dispersive correction as the fitting function in the near wing of the absorption spectrum is well founded by theory since it represents a natural expansion of the collision-broadening rate in terms of the detuning, taking into account the finite duration of the collisions [16,17]. We use fixed, theoretical values for the weight factors  $\beta_{ij}$  and line centers  $\nu_{ij}$  as given in Table I. Due to the high buffer-gas densities we can ignore the Doppler broadening of 0.5 GHz FWHM. The least-squares-fitting procedure allowed for variation of the density shift  $\delta$ , half width  $\sigma$ , asymmetry  $\gamma$ , amplitude (line strength)  $A_a$ , and background  $B_a$  to fit the absorption curve. The maximum error committed using the fitted function for extrapolation in the far wings when calculating the Becquerel spectrum  $\theta_{\text{Becc}}$  was estimated to be smaller than the sys-

TABLE I. Weight factors  $\beta_{ij}$ , centers  $\nu_{ij}$  in gigahertz and summation coefficients  $\lambda_{ij}$  for Eq. (29) for fully resolved lower-state hyperfine structure (lower levels denoted by  $F_g$ ) for the four Rb lines.

Quantity	$^{85}\text{Rb}$ ( $j=1$ )		$^{87}\text{Rb}$ ( $j=2$ )	
	$F_g=2$ ( $i=1$ )	$F_g=3$ ( $i=2$ )	$F_g=1$ ( $i=1$ )	$F_g=2$ ( $i=2$ )
$\beta_{ij}$	0.3006	0.4209	0.1044	0.1741
$\nu_{ij}$ (GHz)	1.680	-1.238	4.155	-2.400
$\lambda_{ij}$	$\frac{4}{45}$	$\frac{8}{45}$	$\frac{1}{15}$	$\frac{1}{5}$

tematic errors due to étalon effects, because the influence from the far wings of the absorption spectrum is extremely small near line center of the Faraday curve. The results of the fits are collected together with results for the Faraday curve and data on temperature, density, and magnetic field in Table II(a) for He buffer gas and in Table II(b) for Xe buffer gas.  $B=1$  indicates that we used the maximum field strength (0.03 T). For illustration some of the results are shown in Fig. 4 as a function of density for He and Xe. In the figure we have fitted straight lines to the measured points in order to guide the eye [18]. Note that the Xe data exhibit a redshift as a function of density, while the He data exhibit a blueshift.

If the Becquerel relation holds, the absorption line shape assumed in Eq. (4) will lead, after a Kramers-Kronig transformation, to a Faraday rotation given directly by Eq. (2),

$$\theta_{\text{Becq}} = A_F \sum_{j=1}^2 \sum_{i=1}^2 \frac{\beta_{ij}(X_{ij}^2 - 1 + 2\gamma_F X_{ij})}{(1 + X_{ij}^2)^2}, \quad (5)$$

$$X_{ij} = \frac{\nu - \nu_{ij} - \delta_F}{\sigma_F},$$

where  $A_F$  is connected to the line strength  $A_a$  by

$$A_F = \alpha \frac{e}{2mc} BL \frac{\nu}{\sigma} A_a \quad (6)$$

and  $\delta_F = \delta$ ,  $\sigma_F = \sigma$ , and  $\gamma_F = \gamma$ . However, by fitting Eq. (5) to the experimental Faraday spectra, using  $A_F$ ,  $\delta_F$ ,  $\sigma_F$ , and  $\gamma_F$  as fit parameters, we find that the optimum fit does not obey the Becquerel relation. It can be seen from Table II, where we have collected the fitting results, that  $\gamma_F$  may deviate as much as 20% from  $\gamma$ ,  $\sigma_F$  up to 10% from  $\sigma$ ,  $\delta_F$  up to 10% from  $\delta$ , and  $A_F$  up to 10% from Eq. (6). In most cases these deviations are significantly larger than the experimental uncertainty. Note also that the differences between the fitted curves using Eq. (5) and the measured Faraday spectra are larger than the experimental uncertainty despite the use of four free fitting parameters. When combined, these observations constitute a proof that we are observing deviations from the Becquerel relation.

In order to quantify the deviations more clearly we project the measured Faraday spectra  $\theta_{\text{Far}}(\nu)$  on the Becquerel spectra  $\theta_{\text{Becq}}(\nu)$ . For this calculation we use the inner product of the spectra determined by integrating their product over the experimental frequency range. We define the projection coefficient as our *scaling factor*  $\alpha_s$

TABLE II. Overview of experimental results from measurements of the absorption and Faraday spectra for (a) Rb:He and (b) Rb:Xe. The spectra are fitted using Eqs. (4) and (5).  $B=1$  indicates that the maximum magnetic field ( $\sim 0.03$  T) was used. The numbers in parentheses after the results indicate  $1\sigma$  statistical error including étalon effects.

[He] or [Xe] ( $10^{19} \text{ cm}^{-3}$ )	$\delta$ (GHz)	$\sigma$ (GHz)	$\gamma$	$\delta_F$ (GHz)	$\sigma_F$ (GHz)	$\gamma_F$	$A_F$ (mrad)	$B$ (relative)	$T$ (K)
(a) Rb:He									
0.32(1)	0.01(3)	1.19(3)	0.004(3)	0.14(6)	1.10(3)	0.34(8)	72.2(20)	0.2	327
0.71(1)	0.13(3)	2.41(5)	0.002(3)	0.00(3)	2.24(5)	0.04(1)	42.7(6)	0.4	336
1.03(2)	0.16(4)	3.52(7)	0.007(4)	-0.27(9)	3.68(7)	-0.12(3)	28.0(3)	0.4	346
2.19(2)	0.36(4)	7.50(13)	-0.006(4)	0.22(4)	7.71(13)	-0.04(1)	30.7(3)	1	352
3.20(3)	0.54(5)	10.97(18)	-0.004(5)	0.40(5)	10.98(18)	0.040(7)	20.18(17)	1	349
4.19(3)	0.41(6)	13.8(2)	-0.026(6)	0.58(6)	14.1(2)	-0.019(7)	15.6(5)	1	361
6.41(4)	0.95(7)	21.2(3)	-0.011(7)	0.96(7)	21.1(3)	-0.026(7)	9.28(8)	1	363
(b) Rb:Xe									
0.33(1)	-0.72(2)	1.17(4)	0.020(5)	-0.59(2)	1.05(2)	0.35(2)	75.1(12)	0.2	333
0.66(1)	-1.52(4)	2.30(4)	0.032(6)	-1.49(3)	2.08(3)	0.15(1)	56.0(7)	0.4	338
1.11(2)	-2.36(4)	3.79(6)	0.076(8)	-2.67(4)	3.89(4)	-0.005(12)	51.7(6)	1	339
2.25(2)	-4.69(6)	7.42(10)	0.116(10)	-4.63(3)	7.54(5)	0.126(3)	27.25(16)	1	348
4.41(3)	-9.29(14)	14.53(18)	0.210(16)	-8.88(6)	14.46(8)	0.237(4)	14.17(8)	1	340
6.00(4)	-13.6(3)	20.6(4)	0.193(18)	-12.14(9)	19.40(12)	0.301(5)	10.21(6)	1	360
7.77(5)	-16.9(2)	25.1(3)	0.318(25)	-15.34(11)	24.82(14)	0.421(6)	6.24(4)	1	360
8.97(6)	-19.1(3)	28.2(4)	0.366(28)	-17.55(12)	28.61(16)	0.472(5)	6.57(4)	1	370

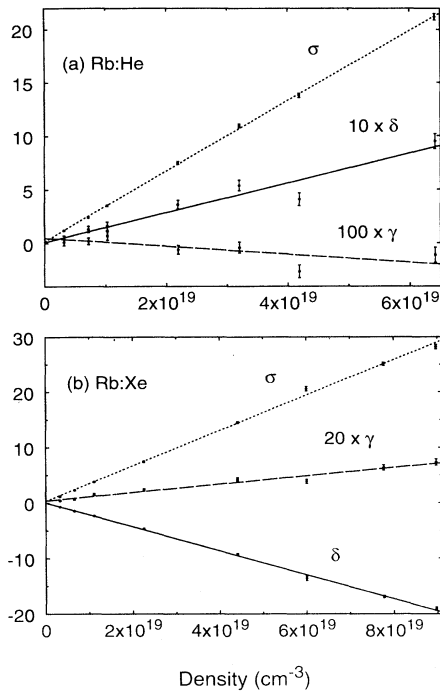


FIG. 4. Experimental results showing  $\sigma$  (GHz),  $\delta$  (GHz), and  $\gamma$  (arbitrary units) from Eq. (4) as a function of density for (a) Rb:He and (b) Rb:Xe. The straight lines are only to guide the eye.

and the remainder of the Faraday spectrum as the *residual spectrum*.

Figure 5 shows a collection of residual spectra for Xe buffer gas. The residual spectra are normalized to the Faraday rotation  $A_F$ , extracted from the fit using Eq. (5). The fully drawn curves give the theoretical results explained in detail in Secs. III and IV. The associated scaling factors are collected in Fig. 6. Again, the curves represent theoretical results explained in Secs. III and IV. The scaling factors vary as a function of buffer-gas density

ty  $\alpha_s = \alpha_s(N)$ , where  $N$  symbolizes [He] or [Xe]. They have been normalized to the theoretical value of  $\alpha_s$  at a relatively low Xe density  $N_0 = 3.3 \times 10^{18} \text{ cm}^{-3}$ . At this low density the scaling factor can be calculated directly, i.e., without violation of the generalized Becquerel relation, as we will show in Sec. III. Thus we effectively calibrate the magnetic field, i.e., we determine the factor  $(eBLv)/(2mc)$  in Eq. (2) to  $\sim 1\%$ . We find theoretically that  $\alpha_s(N_0) = 1.366$ . The value of  $N_0$  has been chosen sufficiently large that we still may neglect Doppler broadening since it is almost one order of magnitude smaller than the pressure broadening. The results obtained with He buffer gas are treated the same way as the Xe results and the same calibration factor is used. These spectra are shown in Figs. 7 and 8. If we had instead used the point measured at  $[\text{He}] = 3.2 \times 10^{18} \text{ cm}^{-3}$  for calibration of  $\alpha_s$ , the result would have deviated less than 1%.

Finally, it is important to consider how the above analysis is influenced by a spatial inhomogeneity of the magnetic field  $B$  and of the Rb concentration  $N_{\text{Rb}}$  inside the cell. For a homogeneous magnetic field the results do not depend on the homogeneity of  $N_{\text{Rb}}$  and not even on the integrated density of Rb,  $\int_0^L N_{\text{Rb}} dz$ , since both the dispersion and the Faraday rotation are proportional to this integral. On the other hand, if  $N_{\text{Rb}}$  is homogeneous inside the cell, the results do not depend on the homogeneity of the magnetic field since the Faraday rotation is then linear in the average magnetic field. However, *both*  $N_{\text{Rb}}$  and  $B$  must be expected to be somewhat spatially inhomogeneous. In this case the absorption is proportional to the averaged Rb density  $\int_0^L N_{\text{Rb}} dz$ , while the Faraday rotation is proportional to the averaged product of Rb density and magnetic field  $\int_0^L N_{\text{Rb}} B dz$ . We will now argue that in our experiments this integral hardly depends on the buffer-gas density. Therefore it will only influence the absolute value of our calibration factor, which anyway we cannot determine accurately in an independent way. The argument goes as follows. We have measured

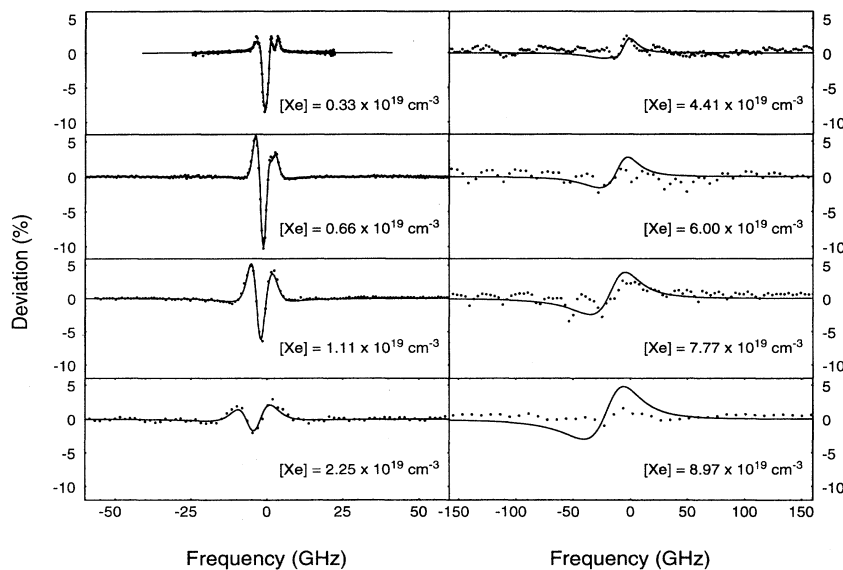


FIG. 5. Dots mark the experimental results for the residual from the Becquerel relation for Rb:Xe. The fully drawn lines indicate the theoretical results for  $\delta' = 1.41 \times 10^{-21} \text{ cm}^3$  and  $\gamma' = 0.25 \times 10^{-21} \text{ cm}^3$ .

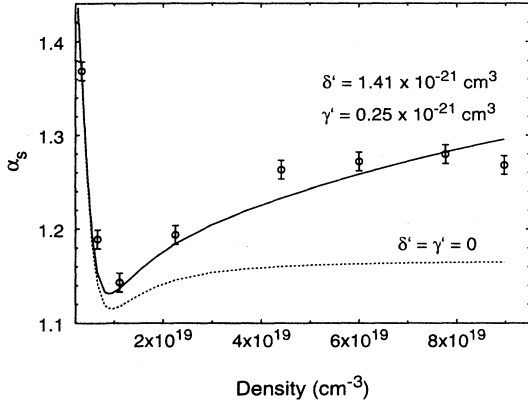


FIG. 6. Scaling factors for Rb:Xe illustrated as circles with error bars. The fully drawn curve is the theoretical result for  $\delta' = 1.41 \times 10^{-21} \text{ cm}^3$  and  $\gamma' = 0.25 \times 10^{-21} \text{ cm}^3$ . The dashed line gives the result for  $\delta' = \gamma' = 0 \text{ \AA}$ , i.e., the Becquerel value generalized for spin and overlapping hyperfine lines.

that the magnetic field has an inhomogeneity of  $\sim 10\%$  within the cell volume probed by the laser, independent of the absolute magnetic field, up to our maximum field strength. The inhomogeneity of  $N_{\text{Rb}}$  is unknown. However, we have good reason to assume that it does not depend on the buffer-gas density. This is based on measurements of  $\int_0^L N_{\text{Rb}} dz$  as a function of buffer-gas density and temperature: For several combinations of temperature, buffer-gas type, and density we find that the integrated Rb density change with temperature is in agreement with the known temperature dependence of the saturated vapor pressure for Rb and that it is independent of buffer-gas density, within the experimental uncertainty. It is unlikely that this would be the case if the inhomogeneity of  $N_{\text{Rb}}$  would depend on buffer-gas density. This leads us to put a conservative upper limit of 5% on buffer-gas density-dependent changes in  $N_{\text{Rb}}$ . Combined with the measured inhomogeneity of the magnetic field we arrive at uncertainties in the final result of  $\sim 0.5\%$ . This is at least two times below the influence of étalon effects.

### III. MAGNETO-OPTICAL LINE-BROADENING THEORY

In this section we derive expressions for the Faraday rotation angle in the specific case of an alkali-metal vapor immersed in a noble gas. We take into account both the hyperfine complication and the onset of quasimolecular complexity. Our starting point is the formalism developed earlier [6]. In that work complications due to hyperfine structure and atomic interactions beyond the impact approximation were neglected. In Ref. [6], as in the present work, we deal with a single fine-structure component. The light frequency is assumed to be near the  $D_2$  transition. Equation (1) gives the Faraday rotation angle in terms of the difference between the refractive index  $n_+$  and  $n_-$  for the two opposite circular polarizations. These refractive indices are matrix elements of the atomic polarizability tensor. The excited state is indicated with the index  $E$  and the ground state with the index  $G$ . The electronic angular momenta of these states are  $J_E = \frac{3}{2}$  and  $J_G = \frac{1}{2}$ . These  $J$  values couple with the nuclear spin  $I$  to yield hyperfine levels indicated by the total angular momentum  $F_e$  and  $F_g$ . We use the lower case letters  $e$  and  $g$  to denote the individual hyperfine levels.

The raising part and the lowering part of the dipole operators between the two states (hyperfine multiplets) are written as  $\mu_{EG}$  and  $\mu_{GE}$ . Each of these parts can be further separated in contributions for each hyperfine transition, so that

$$\mu_{EG} = \sum_{F_e} \sum_{F_g} \mu(F_e F_g). \quad (7)$$

After a slight generalization of the results presented in Ref. [6], the refractive indices  $n_{\pm}$  and the corresponding absorption coefficients  $\kappa_{\pm}$  can be expressed as

$$\begin{aligned} n_{\pm}(\nu) + i\kappa_{\pm}(\nu) \\ = 1 + \frac{N_{\text{Rb}}}{2\epsilon_0} \sum_{F_e, F_g} \sum_{F'_e, F'_g} \frac{2\pi i}{h} \text{Tr} \{ \mu_{\pm}(F'_g F'_e) K(\nu) \\ \times [\mu_{\pm}(F_e F_g) \rho(F_g)] \}, \end{aligned} \quad (8)$$

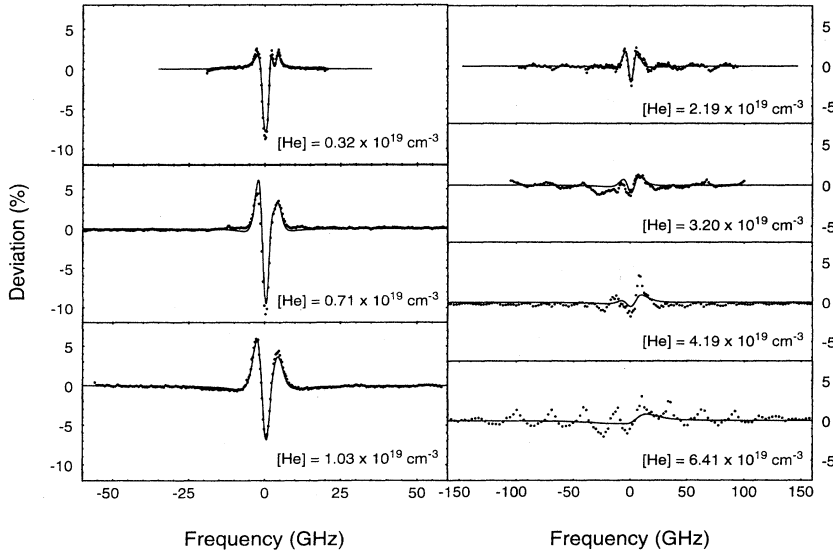


FIG. 7. Dots mark the experimental results for the residual from the Becquerel relation for Rb:He. The fully drawn lines indicate the theoretical results for  $\delta' = 6.9 \times 10^{-22} \text{ cm}^3$  and  $\gamma' = 1.6 \times 10^{-22} \text{ cm}^3$ .

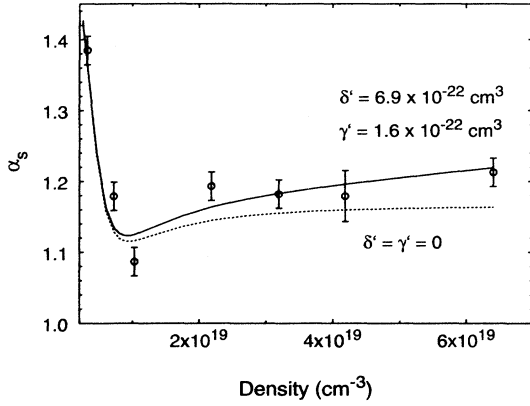


FIG. 8. Scaling factors for Rb:He illustrated as circles with error bars. The fully drawn curve is the theoretical result for  $\delta' = 6.9 \times 10^{-22} \text{ cm}^3$  and  $\gamma' = 1.6 \times 10^{-22} \text{ cm}^3$ . The dashed line gives the result for  $\delta' = \gamma' = 0 \text{ \AA}$ , i.e., the Becquerel value generalized for spin and overlapping hyperfine lines.

where we have introduced the partial dipole components along the circular polarization vectors

$$\mu_{\pm}(F_e F_g) = \mathbf{\mu}(F_e F_g) \cdot \mathbf{u}_{\pm}, \quad \mu_{\pm}(F_g F_e) = \mu_{\pm}^{\dagger}(F_e F_g), \quad (9)$$

where  $\mathbf{u}_{\pm}$  are the polarization vectors for the two circular polarizations. The operator  $K$ , which acts on atomic operators, is defined in terms of a collision operator  $\Phi(\nu)$  as

$$K(\nu) = \frac{1}{\Phi(\nu) + i(L - 2\pi\nu)}, \quad (10)$$

where  $\Phi(\nu)$  describes the effect of a binary collision of the active atom with a buffer gas particle. The partial density matrix  $\rho(F_g)$  of the atoms in the hyperfine ground level  $F_g$  is assumed to be isotropic, since optical pumping is neglected. The Liouville operator  $L$  denotes the commutator with the Hamiltonian of a single atom, including the hyperfine and Zeeman splitting. We separate  $L$  as

$$L = L_0 + L_1, \quad (11)$$

where  $L_0$  contains the transition frequencies of the atom and  $L_1$  describes the Zeeman effect. When operating on the partial dipole operators  $\mu_{\pm}(F_e F_g)$ ,  $L_0$  gives

$$L_0 \mu_{\pm}(F_e F_g) = 2\pi\nu(F_e F_g) \mu_{\pm}(F_e F_g), \quad (12)$$

with  $\nu(F_e F_g)$  the transition frequencies between the hyperfine levels. Restricted to a single fine-structure component, the Zeeman term  $L_1$  is defined by the equality

$$L_1 \mu_{EG} = \frac{\pi e B}{mh} [g_E J_z \mu_{EG} - g_G \mu_{EG} J_z] \quad (13)$$

with

$$g_E, g_G = 1 + \frac{J(J+1) - L(L+1) + S(S+1)}{2J(J+1)}, \quad (14)$$

the Landé factors of the two states. For the  $D_2$  transition we have  $g_G = 2$  and  $g_E = \frac{4}{3}$ . Finally, the collision operator

$\Phi(\nu)$  is proportional to the density of the buffer gas particles and it can be expanded as

$$\Phi(\nu) = \Phi_0(\nu) + \Phi_1(\nu), \quad (15)$$

with  $\Phi_0$  the collision operator in the absence of the magnetic field and  $\Phi_1$  its first-order correction in the magnetic field. An explicit but formal expression for  $\Phi_0$  is well known in the ULB theory [11], but it is immaterial for our present purpose. Generalization of this expression to include the Zeeman Liouvillian operator  $L_1$  is straightforward. It leads to an equally formal and explicit expression for  $\Phi_1$ .

Expansion of  $K(\nu)$  to first order in the Zeeman term gives the result

$$K(\nu) = K_0(\nu) - K_0(\nu) [\Phi_1(\nu) + iL_1] K_0(\nu), \quad (16)$$

where  $K_0(\nu)$  is given by an expression similar to Eq. (10), with  $\Phi$  and  $L$  replaced by  $\Phi_0$  and  $L_0$ . Because of the isotropy of the unperturbed sample, the operator  $\Phi_0$  is a scalar operator. Moreover, since the duration of a collision is small compared to the hyperfine precession time, this operator does not act on the nuclear spin, but exclusively on the electronic degrees of freedom. Therefore, the raising part of the dipole operator  $\mu_{EG}$  must be an eigenvector of  $\Phi_0$ . This implies that the partial dipole operators  $\mu_{\pm}(F_e F_g)$  are eigenvectors of  $K_0(\nu)$  and we write

$$K_0(\nu) \mu_{\pm}(F_e F_g) = k_0[\Delta(F_e F_g)] \mu_{\pm}(F_e F_g). \quad (17)$$

The complex eigenvalue  $k_0(\Delta(F_e F_g))$  depends on the hyperfine levels  $F_e$  and  $F_g$  only through the detuning

$$\Delta(F_e F_g) = \nu - \nu(F_e F_g) \quad (18)$$

of the light frequency from the hyperfine transition. The function  $k_0(\Delta(F_e F_g))$  has the ULB absorption profile of the line  $F_g \rightarrow F_e$  as its real part, while its imaginary part is the corresponding dispersion curve. These real and imaginary parts are related by Kramers-Kronig relations. For low noble-gas densities, when the line core is described by the impact limit, the functions  $k_0$  take a Lorentzian form. However, our measured absorption profiles are highly asymmetric so it is necessary to include a more general expression for  $k_0$ . This can be done by adding an asymmetric contribution in the numerator, with the result

$$k_0(\Delta(F_e F_g)) = \frac{1 + i\gamma}{2\pi[\sigma + i\delta - i\Delta(F_e F_g)]} \quad (19)$$

with  $\sigma$  the collisional width,  $\delta$  the collisional shift, and  $\gamma$  parametrizing the line asymmetry. This is analogous to an expansion of the collisional width to first order in the product of detuning and the inverse duration of the collisions  $\tau^{-1}$  introduced by others [16,17]. The expressions (4) and (5) previously given for the absorption profile and Faraday rotation according to Becquerel directly follow from Eq. (19) by taking the real and the imaginary part.

The expansion of the refractive indices  $n_{\pm}$  in the magnetic field follows after expanding Eq. (10) and substitut-

ing the result in Eq. (8). For the refractive index and the absorption coefficient to zeroth order in the magnetic field we find, with Eq. (17),

$$n_0(\nu) + i\kappa_0(\nu) = 1 + \frac{N_{\text{Rb}}}{2\epsilon_0} \sum_{F_e, F_g} \frac{2\pi i}{h} k_0(\Delta(F_e F_g)) \text{Tr}[\mu_{\pm}(F_g F_e) \mu_{\pm}(F_e F_g) \rho(F_g)] . \quad (20)$$

Because of the isotropy of  $\rho(F_g)$  this expression does not depend on the polarization. The first-order correction is

$$n_{1\pm}(\nu) + i\kappa_{1\pm}(\nu) = -\frac{N_{\text{Rb}}}{2\epsilon_0} \sum_{F_e, F_g} \sum_{F_e', F_g'} \frac{2\pi i}{h} k_0(\Delta(F_e' F_g')) k_0(\Delta(F_e F_g)) \text{Tr}\{\mu_{\pm}(F_g' F_e') [\Phi_1 + iL_1] [\mu_{\pm}(F_e F_g) \rho(F_g)]\} . \quad (21)$$

For symmetry reasons, these corrections for opposite circular polarization are each other's opposite [6].

So far, the calculation has been exact to first order. The generalized Becquerel relation follows from the assumption that the Zeeman term  $L_1$  simply acts as a frequency shift so we may make the substitution

$$\Phi_1 = -\frac{1}{2\pi} \frac{\partial \Phi_0}{\partial \nu} L_1 \quad (22)$$

with  $\Phi_0$  defined by Eq. (17) through the operator equality

$$\Phi_0 = \frac{1}{K_0(\nu)} - i(L_0 - 2\pi\nu) . \quad (23)$$

It may be shown that the substitution for  $\Phi_1$  in Eq. (22) is exact when the atom-perturber interaction is fully isotropic, so that it commutes with the Zeeman operator  $L_1$  [20]. In the case of an asymmetric line ( $\gamma \neq 0$ ) an expression for the derivative operator  $\partial \Phi_0 / \partial \nu$  is obtained after substituting Eq. (19) into Eq. (17) and taking the frequency derivative of both sides. The derivative operator then gives  $-2\pi\gamma / (1+i\gamma)$  when acting on a raising dipole  $\mu_{\pm}(F_e F_g)$ . Allowing for a deviation from the generalized Becquerel relation we write

$$\Phi_1 \mu_{\pm}(F_e F_g) = \frac{\gamma}{1+i\gamma} L_1 \mu_{\pm}(F_e F_g) + \Phi'_1 \mu_{\pm}(F_e F_g) , \quad (24)$$

where  $\Phi'_1$  arises from the noncommutativity of the Zeeman term with the collisional interaction and describes deviations from the generalized Becquerel relation.

The result can be further simplified if we use the fact that the density of the noble gas is sufficiently high so the hyperfine splitting of the excited state is smaller than the

collisional width. Then the dependence of the detuning  $\Delta$  on the excited hyperfine level  $F_e$  can be ignored. However, we still allow  $\Delta$  to depend on the ground-state hyperfine level and the corresponding functions  $k_0$  are simply indicated as  $k_0(F_g)$ . A second simplification arises from the fact that the interaction between a noble-gas atom and an alkali-metal atom in the ground-state is governed by a single potential curve, so that this interaction is fully isotropic. This implies that the Zeeman term cannot perturb the effect of a ground-state collision and conversely, the Zeeman precession in the ground state is not hindered by the collisional interaction. Therefore, the perturbation  $\Phi'_1$  can only affect the excited state. Because of the symmetry of the Zeeman term, this perturbation has a vector character and we can parametrize  $\Phi'_1$  acting on a partial dipole operator as

$$\Phi'_1 \mu_{\pm}(F_e F_g) = \frac{\pi e B}{m h} \phi' J_z \mu_{\pm}(F_e F_g) , \quad (25)$$

with  $\phi'$  a complex number. The real part of  $\phi'$  determines the Zeeman correction to the collisional width and its imaginary part gives the correction to the shift. One should recall that  $\phi'$  is proportional to the density  $N$  of the noble gas. We parametrize  $\phi'$  as  $\phi' = (\gamma' + i\delta')N$ , where  $\delta', \gamma'$  are small parameters of order  $2\pi\sigma\tau/N$ . After these approximations, the first-order corrections to the refractive index can be explicitly evaluated by using standard angular momentum algebra. If we use the fact that the mathematical consequence of the Becquerel contribution to  $\Phi_1$  [the first term in Eq. (24)] is merely a division of the  $g$  factors by  $(1+i\gamma)$ , we get the magnetic corrections to the refractive index

$$\begin{aligned} n_{1\pm}(\nu) = & \pm \frac{A_a}{2I+1} \left[ \sum_{F_g} \frac{2F_g+1}{2J_g+1} [2+J_e(J_e+1)-J_g(J_g+1)] \text{Re} \left[ k_0^2(F_g) \left( \frac{g_E}{1+i\gamma} - i\phi' \right) \right] \right. \\ & + \sum_{F_g} \sum_{F_g'} [2+J_g(J_g+1)-J_e(J_e+1)] (2F_g+1)(2F_g'+1) \left. \left\{ \begin{matrix} J_g & J_g & 1 \\ F_g & F_g' & I \end{matrix} \right\}^2 \frac{g_G}{1+i\gamma} \right. \\ & \left. \left. \times \text{Re}[k_0(F_g)k_0(F_g')] \right] \right] \frac{\pi e B}{4m} \sigma . \quad (26) \end{aligned}$$

The overall strength factor  $A_a$  is

$$A_a = \frac{N_{\text{Rb}}}{6\epsilon_0 h \sigma} \frac{1}{2J_g + 1} |\langle J_e \| \mu \| J_g \rangle|^2 \quad (27)$$

in terms of the reduced dipole moment of the transition which obeys the relation

$$\text{Tr}[\mu_{\pm}(F_g F_e) \mu_{\pm}(F_e F_g) \rho(F_g)] = \frac{1}{3} |\langle J_e \| \mu \| J_g \rangle|^2. \quad (28)$$

The strength factor  $A_a$  is identical to the strength factor used in Eq. (4) for fitting the absorption line shapes. For comparison with experiments the contributions from the two isotopes  $^{85}\text{Rb}$  and  $^{87}\text{Rb}$  must be added in Eq. (26).

This result determines the Faraday rotation angle as a function of the frequency  $\nu$ . It generalizes the result for a single fine-structure component [6] in three ways. First,

$$\theta_{\text{Far}} = \sum_{j=1}^2 \sum_{i=1}^2 \beta_{ij} \left[ \frac{(\frac{4}{3} - \lambda_{ij} + N\delta')(X_{ij}^2 - 1) + 2[(\frac{4}{3} - \lambda_{ij})\gamma - N\gamma']X_{ij}}{(1 + X_{ij}^2)^2} - \left[ \frac{2}{5} - \lambda_{ij} \right] \frac{X_{ij}X_{(3-i)j} - 1 + \gamma(X_{ij} + X_{(3-i)j})}{(1 + X_{ij}^2)(1 + X_{(3-i)j}^2)} \right] \frac{5}{4} \frac{\nu}{\sigma} A_a \frac{e}{2mc} BL, \quad X_{ij} = \frac{\nu - \nu_{ij} - \delta}{\sigma}, \quad (29)$$

where the parameters  $\beta_{ij}$ ,  $\lambda_{ij}$ , and  $\nu_{ij}$  have been given in Table I and  $\delta'$ ,  $\gamma'$  are small parameters of order  $2\pi\sigma\tau/N$ . The connection between  $\delta'$ ,  $\gamma'$  and  $\phi'$  is given by  $\phi' = (\gamma' + i\delta')N$ , where  $N$  is the density of the noble gas. It is informative to consider Eq. (29) in the limit where  $\delta' = \gamma' = 0$  so there are no deviations from the generalized Becquerel relation. In the high-density limit [ $\sigma \gg (\nu_{ij} - \nu_{i'j'})$ ] Eq. (29) then reduces to Eqs. (5) and (6) with  $\alpha = \frac{7}{6}$ . This result for  $\alpha$  can also be found using simple angular momentum coupling [5]. In the low-density limit [ $\sigma \ll (\nu_{ij} - \nu_{i'j'})$ ] Eq. (29) corresponds to Eq. (2) with four different values of  $\alpha$  for the four individual hyperfine lines. These values are  $\frac{14}{9}$  ( $F_g = 2$ ) and  $\frac{13}{9}$  ( $F_g = 3$ ) for  $^{85}\text{Rb}$  and  $\frac{19}{12}$  ( $F_g = 1$ ) and  $\frac{17}{12}$  ( $F_g = 2$ ) for  $^{87}\text{Rb}$  leading to violation of Eq. (5). In general the expression (5) for the Faraday spectrum is only correct when all hyperfine splittings are small compared to the collisional linewidth and quasimolecular deviations from the Becquerel relation are negligible.

We use the expression given by Eq. (29) to make a least-squares fit to all experimental spectra obtained for one buffer gas. In this way we find  $|\phi'|/[\text{He}] = (7.1 \pm 2.9) \times 10^{-22} \text{ cm}^3$  for He buffer gas. For Xe buffer gas we find  $|\phi'|/[\text{Xe}] = (1.4 \pm 0.4) \times 10^{-21} \text{ cm}^3$ . The fit obtained in this way is generally better than the fit obtained with Eq. (5) despite that we have only two free parameters instead of four and that the fit is made to a whole series of spectra instead of only one spectrum.

We have previously determined  $|\phi'|$  for Xe buffer gas in a slightly different way [9]. We used an expression similar to Eq. (29), but included two higher-order terms proportional to  $-4\gamma\gamma'(x^2 - 1)/(1 + x^2)$  and  $2\gamma\delta'x/(1 + x^2)$ , respectively. Hereby we found a better fit to the data with  $|\phi'|/[\text{Xe}] = (3.6 \pm 0.5) \times 10^{-21} \text{ cm}^3$ .

the hyperfine splitting is explicitly included. Second, the line profiles may differ from their behavior in the impact limit. Third, perturbation of the Zeeman precession by binary collisions during the precession is accounted for. This effect is expressed by the complex parameter  $\phi'$ . If  $\phi' = 0$ , Eq. (26) leads to the generalized Becquerel relation for the Rb  $D_2$  transition.

#### IV. COMPARISON OF EXPERIMENTAL RESULTS WITH LINE-BROADENING THEORY

A general expression for the Faraday rotation taking into account, within the binary collision approximation, the influence of nuclear spin and quasimolecular effects follows from Eq. (26) combined with Eq. (1). To first order in  $2\pi\sigma\tau$  the Faraday rotation can then be written as

However, these two terms are quadratic instead of linear in density and are therefore inconsistent with a binary collision treatment within the ULB theory as given in Sec. III. The fact that the inclusion of these terms leads to improved agreement with the measurements is therefore an indication that we are observing effects of multiple collisions. This invalidates our previous conclusion [9] that the binary collision approximation ( $2\pi\sigma\tau \ll 1$ ) holds true for higher densities than expected. In fact, for our highest Xe pressure (4 atm) we have  $2\pi\sigma\tau \sim 1$  since  $\tau = \rho_W/\nu \sim 5 \times 10^{-12} \text{ s}$ , where  $\rho_W$  is the Weisskopf radius [5,12].

For the phase angle  $\arg(\phi')$ , we measure  $(77 \pm 8)^\circ$  for He buffer gas and  $(80 \pm 7)^\circ$  for Xe buffer gas. These angles are equal within the experimental uncertainty. This might be an indication that the ratio of  $\delta'$  and  $\gamma'$  is more dependent on properties of the Rb atom than on properties of the perturbing buffer-gas atoms. On the contrary, the absolute value  $|\phi'|$  is sensitive to the nature of the buffer gas. The deviations from the Becquerel relation calculated with these two values of  $\phi'$  are illustrated as fully drawn curves in Figs. 5–8. The agreement with the experimental results is good, except for the systematic trend for the experimental scaling factors for Rb:Xe to bend downward at the highest densities. For comparison we have plotted the results obtained with  $\phi' = 0$  as dashed curves in Figs. 6 and 8. All curves (including those for  $\phi' = 0$ ) show a minimum for  $\alpha_s$  near a density of  $8 \times 10^{18} \text{ cm}^{-3}$ . This is due to a coherence between ground-state hyperfine levels, which manifests itself theoretically as a negative sign in front of the second term within the large square brackets in Eq. (29). The maximum absolute violation of the Becquerel relation is approximately 9% for some of the higher Xe pressures (see Fig. 6). Note

that the Faraday effect is *larger* than its Becquerel value. At higher densities we expect the Faraday effect to decrease below its Becquerel value in line with a classical picture of locking. The downward bend at the highest Xe density is probably the first indication of this later decrease.

For the same buffer-gas density the deviations from the Becquerel relation are smaller for He compared to Xe, roughly by a factor of 2 (see Figs. 6 and 8 and Table II). This difference is in qualitative agreement with expectations based on the collision dynamics in the gas mixture.

### V. COLLISION PHYSICS PICTURE

We will now discuss the collisional dynamics of the alkali-metal–noble-gas systems and point out a close connection between “microscopic” collisional properties in the gas mixtures and our “macroscopic” line-broadening results. Consider as an example an isolated, binary collision between a  $^1S$  state perturber atom and a probe atom with a  $^1S$  ground state and a  $^1P$  excited state connected by an optical transition, as illustrated in Fig. 9. If the electrostatic interaction between the two atoms has only a weak angular dependence, the excited  $p$  state maintains its orientation due to electronic inertia [Fig. 9(a)]. If the electrostatic interaction has a strong angular dependence, the corresponding torque orients the  $p$  state along the internuclear axis [Fig. 9(b)]. Thus angular coupling takes place when the electrostatic splitting  $(V_{\Sigma} - V_{\Pi})/\hbar$  of the  $p$  state exceeds the angular velocity  $v/R$  [21,22],

$$|V_{\Sigma} - V_{\Pi}| \geq \hbar \frac{v}{R}, \quad (30)$$

where  $V_{\Sigma}(R)$  and  $V_{\Pi}(R)$  are adiabatic potentials and  $R$  is the internuclear distance. Solving the inequality (30) for  $R$  leads to  $R \leq R_{\text{lock}}$ , where  $R_{\text{lock}}$  is the locking radius. For distances smaller than  $R_{\text{lock}}$  the  $p$  state and thereby the electric dipole moment responsible for the  $S$ - $P$  transition becomes locked to the internuclear axis. The same takes place for the magnetic dipole moment of the  $p$  state leading to modification of the magnetic precession. This argument is not limited to the special case of singlet states. For multiplet states it is the total angular momentum  $J$  that may lock to the collision axis, again depending

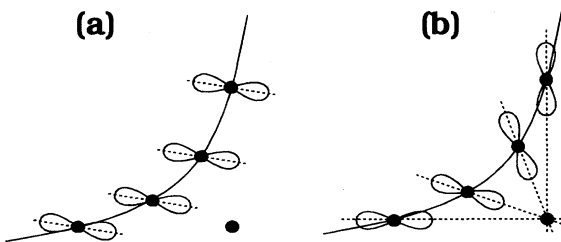


FIG. 9. The evolution of an electronic  $p$  state during a collision with an  $s$ -state perturber. When electronic inertia dominates (a) the wave function is fixed in the laboratory frame; when angular coupling dominates (b) the  $p$  state is locked to the collisional axis.

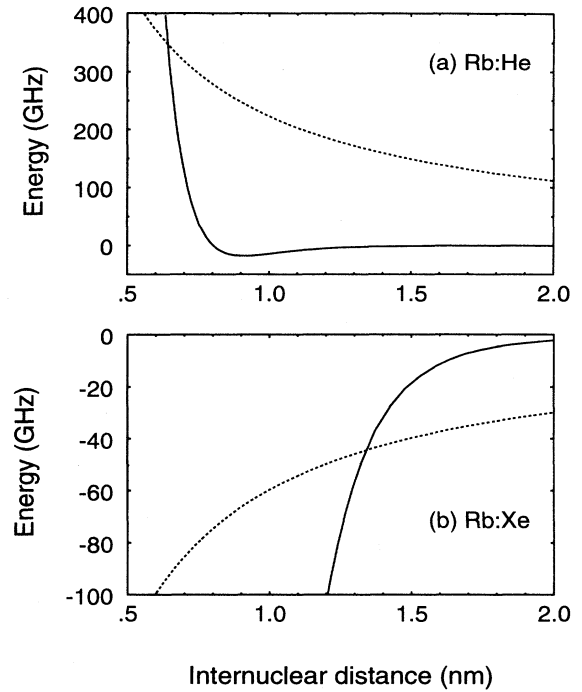


FIG. 10. Illustration of how to determine  $R_{\text{lock}}$  for (a) Rb:He and (b) Rb:Xe. The fully drawn curves are the potential differences  $V_{\Sigma} - V_{\Pi}$  from Pascale and Vandephanque [23]. The dashed curves correspond to  $\pm \hbar v/R$ . Locking occurs when a dashed curve crosses a fully drawn curve.

on the energy splitting between the differently oriented electron orbitals. We can therefore use Eq. (30) to determine  $R_{\text{lock}}$  for the Rb noble-gas systems. Using the theoretical potentials by Pascale and Vandephanque [23] we find  $R_{\text{lock}} = 6.4 \text{ \AA}$  for Rb:He and  $R_{\text{lock}} = 13.4 \text{ \AA}$  for Rb:Xe, as illustrated in Fig. 10.

The spectroscopic interpretation of the inequality (30) is that  $V_{\Sigma}$  and  $V_{\Pi}$  correspond to line shifts and splittings (assuming  $V = 0$  for the ground state) and  $\hbar v/R$  is the bandwidth of the radiation absorbed or emitted during a collision. If inequality (30) is satisfied, a gas-phase atom always “feels” a (time-dependent) axis; it corresponds to the invalidity of the impact approximation at line center and the onset of quasistatic behavior associated with violations of the Becquerel relation.

Both  $\delta'$  and  $\gamma'$  have the dimension of a volume. It seems natural to interpret this volume as that within which locking occurs, leading to deviations from the single-atom behavior of the electronic transitions and thereby violation of the Becquerel relation. From this dimensional argument one would therefore expect that  $|\phi'|/N = |\gamma' + i\delta'| \sim R_{\text{lock}}^3$ . For Rb:He we thus estimate  $|\phi'|/[\text{He}] \sim 1 \times 10^{-21} \text{ cm}^3$ , which is consistent with the experimental result  $7.1 \times 10^{-22} \text{ cm}^3$ . For Rb:Xe we estimate  $|\phi'|/[\text{Xe}] \sim 1 \times 10^{-20} \text{ cm}^3$ , which is larger than the experimental result  $1.4 \times 10^{-21} \text{ cm}^3$ . This deviation may well be due to the influence of multiperturber effects in Xe buffer gas: the average distance from a Rb atom to the nearest Xe neighbor becomes comparable to  $R_{\text{lock}}$  at

our highest Xe densities. For  $[\text{Xe}] = 8.97 \times 10^{19} \text{ cm}^{-3}$  we find an average Rb-Xe distance of 13.9 Å, which is almost identical to  $R_{\text{lock}}$ . This means that there will be two or more Xe atoms within  $R_{\text{lock}}$  for a substantial fraction of the time. This is expected to give rise to considerable modification of the locking due to nonadditivity aspects.

## VI. CONCLUSION

In conclusion, we have observed substantial violation of the generalized Becquerel relation for the Faraday effect of Rb atoms in Xe buffer gas. For He buffer gas the quasimolecular violations are approximately two times smaller than for Xe. Both systems show the same ratio between  $\delta'$  and  $\gamma'$  leading to a phase angle for  $\phi'$  of approximately 79°. Theoretical values for  $\delta'$  and  $\gamma'$  are not yet available. Therefore our magneto-optical line-broadening theory is only a parametrization so far. Note that this parametrization does not even predict the sign of the Becquerel violation. A direct calculation of  $\phi'$  should be possible using the ULB theory and available Rb noble-gas potentials [23]. It would then be interesting to see whether the binary ULB approach gives the correct quantitative result for  $\delta'$  and  $\gamma'$ . We would expect this to be the case for the Rb:He system, but not necessarily for the Rb:Xe system due to the influence of

multiperturber effects.

The extraction of the quasimolecular deviations from the Becquerel relation from the data is technically complicated due to the presence of hyperfine structure in the Rb spectrum. It would have been easier to investigate a system without hyperfine structure, although suitable candidates have other disadvantages. Presently we are investigating the Faraday effect of Rb in noble gases at higher densities, where the hyperfine-structure complications become irrelevant.

Our results constitute a link between the spectroscopically observed Faraday effect and collision physics. So far we have observed the onset of quasimolecular aspects at gas-phase densities up to  $\sim 10^{20} \text{ cm}^{-3}$  in Xe buffer gas. At higher gas densities we expect to see complete development toward condensed-matter behavior of the Faraday effect. At sufficiently high density the multiperturber effects should become dominant, probably leading to drastic modifications of the Faraday effect.

## ACKNOWLEDGMENTS

This work is part of the research program of the Foundation for Fundamental Research on Matter (FOM) and was made possible by financial support from the Netherlands Organization for Scientific Research (NWO).

- 
- [1] L. D. Barron, *Molecular Light Scattering and Optical Activity* (Cambridge University Press, Cambridge, 1982).
  - [2] Z. Wu, M. Kitano, W. Happer, M. Hou, and J. Daniels, *Appl. Opt.* **25**, 4483 (1986).
  - [3] M. E. Wagshul and T. E. Chupp, *Phys. Rev. A* **49**, 3854 (1994).
  - [4] H. Becquerel, *C. R. Acad. Sci. Paris* **125**, 697 (1897).
  - [5] J. P. Woerdman, G. Nienhuis, and I. Kuščer, *Opt. Commun.* **93**, 135 (1992).
  - [6] G. Nienhuis, J. P. Woerdman, and I. Kuščer, *Phys. Rev. A* **46**, 7079 (1992).
  - [7] G. Herzberg, *Spectra of Diatomic Molecules* (Van Nostrand, Princeton, 1957).
  - [8] R. Serber, *Phys. Rev.* **41**, 489 (1932).
  - [9] M. Kristensen, M. A. van Eijkelenborg, and J. P. Woerdman, *Phys. Rev. Lett.* **72**, 2155 (1994).
  - [10] A. Gallagher, *Phys. Rev.* **157**, 68 (1967); R. G. Breene, Jr., *Theories of Spectral Line Shapes* (Wiley, New York, 1981).
  - [11] E. W. Smith, J. Cooper, and L. J. Roszman, *J. Quant. Spectrosc. Radiat. Transfer* **13**, 1523 (1973).
  - [12] E. L. Lewis, *Phys. Rep.* **58**, 1 (1980).
  - [13] E. Milani, *Appl. Opt.* **32**, 5217 (1993).
  - [14] W. Happer, *Rev. Mod. Phys.* **44**, 169 (1972).
  - [15] Y. C. Chan and J. A. Gelbwachs, *J. Phys. B* **25**, 3601 (1992).
  - [16] J. Szudy and W. E. Baylis, *J. Quant. Spectrosc. Radiat. Transfer* **15**, 641 (1975).
  - [17] R. E. Walkup, A. Spielfiedel, and D. E. Pritchard, *Phys. Rev. Lett.* **45**, 986 (1980).
  - [18] Naively, one would, within a binary collision theory, expect the points to lie on straight lines. But this is not always true in reality. As an example we comment on the ratio of the shift to the width (i.e.,  $\delta/\gamma$ ) of the pressure-broadened transition. One would normally assume this ratio to be independent of density in the regime where our experiments are performed [15]. For He buffer gas this indeed seems to be true within the  $\sim 10\%$  experimental uncertainty for the individual points. For Xe buffer gas the relative experimental uncertainty on the ratio  $\delta/\gamma$  is substantially smaller. From the Rb:Xe data in Fig. 4 it follows that the ratio shows a slight, but significant, decrease with increasing pressure and temperature. However, it remains close to the value  $-0.72$  expected for a pure van der Waals potential. We think that the systematic decrease may be due to the temperature dependence predicted by Hindmarsh, Petford, and Smith for the special case of a Lennard-Jones potential [19]. However, it may also be partly related to multiple Xe perturbers present around each Rb atom.
  - [19] W. R. Hindmarsh, A. D. Petford, and G. Smith, *Proc. R. Soc. London Ser. A* **297**, 296 (1967).
  - [20] G. Nienhuis and S. Kryszewski, *Phys. Rev. A* **50**, 5051 (1994).
  - [21] J. Grosser, *Comments At. Mol. Phys.* **21**, 107 (1988).
  - [22] W. J. Alford, N. Andersen, K. Burnett, and J. Cooper, *Phys. Rev. A* **30**, 2366 (1984).
  - [23] J. Pascale and J. Vandeplanque, *J. Chem. Phys.* **60**, 2278 (1974); J. Pascale and J. Vandeplanque, CEA Report Service de Physique Atomique, Saclay, March 1974 (unpublished).